catalysts

MDPI

Review

Modified Catalysts and Their Fractal Properties

Gianina Dobrescu [1,*], Florica Papa [1,*], Razvan State [1], Monica Raciulete [1], Daniela Berger [2], Ioan Balint [1] and Niculae I. Ionescu [1]

[1] Surface Chemistry and Catalysis Laboratory, "Ilie Murgulescu" Institute of Physical-Chemistry of the Romanian Academy, 202 Spl. Independentei, 060021 Bucharest, Romania; rstate@icf.ro (R.S.); mpavel@icf.ro (M.R.); ibalint@icf.ro (I.B.); ionescu@icf.ro (N.I.I.)

[2] Faculty of Applied Chemistry and Materials Science, University Politehnica of Bucharest, 1-7 Gheorghe Polizu St., 011061 Bucharest, Romania; daniela.berger@upb.ro

* Correspondence: gdobrescu@icf.ro (G.D.); frusu@icf.ro (F.P.)

Abstract: Obtaining high-area catalysts is in demand in heterogeneous catalysis as it influences the ratio between the number of active surface sites and the number of total surface sites of the catalysts. From this point of view, fractal theory seems to be a suitable instrument to characterize catalysts' surfaces. Moreover, catalysts with higher fractal dimensions will perform better in catalytic reactions. Modifying catalysts to increase their fractal dimension is a constant concern in heterogeneous catalysis. In this paper, scientific results related to oxide catalysts, such as lanthanum cobaltites and ferrites with perovskite structure, and nanoparticle catalysts (such as Pt, Rh, Pt-Cu, etc.) will be reviewed, emphasizing their fractal properties and the influence of their modification on both fractal and catalytic properties. Some of the methods used to compute the fractal dimension of the catalysts (micrograph fractal analysis and the adsorption isotherm method) and the computed fractal dimensions will be presented and discussed.

Keywords: fractal dimension; modified catalysts; fractal analysis; perovskite; nanoparticles

Citation: Dobrescu, G.; Papa, F.; State, R.; Raciulete, M.; Berger, D.; Balint, I.; Ionescu, N.I. Modified Catalysts and Their Fractal Properties. *Catalysts* **2021**, *11*, 1518. https://doi.org/10.3390/catal11121518

Academic Editor: Bruno Fabre

Received: 10 November 2021
Accepted: 11 December 2021
Published: 14 December 2021

1. Introduction

The power of self-similarity as a fractal property was first emphasized in 1975 by B.B Mandelbort [1,2]. Following this finding, many processes and phenomena were analyzed as fractal behavior: light scattering on rough surfaces [3], fractal antennae [4], diffusion-limited aggregation [5], fractures [6], reaction kinetics [7], tumor diagnosis and cancer therapy [8,9] and, recently, mechanical responses of cell membranes [10].

In 1984, David Avnir, Dina Farin and Peter Pfeifer [11] reported that, at the molecular scale, the surfaces of most materials are fractal. This property leads to scaling laws of great interest in the description of various processes specific to heterogeneous chemistry: physical adsorption, chemisorption, and catalytic processes. Lately, a series of articles regarding the fractal analysis of surfaces of some catalysts and catalytic reactions have appeared in literature [12–26].

Tailoring catalysts with high activity in specific reactions is a challenging field of interest. Strategies implying the influence of particle size on catalytic properties [27] or metal-support interaction [28] or morphological controlling, metal deposition and chemical treatment [29] are largely seen in the literature. In the following, we shall focus only on the influence of fractal behavior self-similarity on catalytic properties.

Briefly, from a geometric point of view, catalytic reactions are favored by the existence of a large number of active centers arranged on the irregular surfaces of the catalysts, surfaces that have large specific surface areas (BET). Therefore, the surface of a catalyst can't be described as a flat surface, but rather as a sum of convoluted flat surfaces. Thus, fractal geometry can describe the surface of a catalyst better than classic, Euclidean geometry. Fractal geometry deals with the description of certain properties and characteristics of

catalysts as scale sizes, not as their sums for small entities, keeping the same mathematical properties at different scales.

Not every random structure is fractal [1,2]: it is necessary to verify the existence of the self-similarity property on a sufficiently large scaling area to be able to conclude that the object itself is fractal.

The characterization of a fractal object is related to the measurement of two properties: the fractal dimension and the scaling domain. The fractal dimension, which is often a fractional number between 2 and 3 for surfaces, and, respectively, between 1 and 2 for powders, measures the degree of space occupancy, irregularity and roughness, and becomes close to three for surfaces that tend to "fill" the entire volume and two for surfaces that tend towards the plane, while the domain of self-similarity is the scaling area where the fractal properties are manifested [1,2]. The greater the field of self-similarity, the closer the fractal gets to an ideal mathematical fractal.

This work's focus is our results regarding the fractal characterization of oxide catalysts with perovskite structure (cobaltite and ferrite), as well as of some supported and unsupported metallic nanoparticles (NP) of Pd, Pt, Rh and bimetallic Pd-Cu, Pd-Ag and Pt-Cu. The fractal characteristics of these catalysts will be correlated with their catalytic properties. Fractal analysis will be performed both by SEM or TEM image analysis of micrographs and by the nitrogen adsorption isotherms method.

Therefore, based on the analyzed catalytic materials, the present paper aims to highlight the fractal character of various investigated catalysts and the means in which the fractal characteristics are tailored based on the modified catalysts. The impact on the catalytic properties will also be emphasized.

2. Results

2.1. Influences of Synthesis Parameters on the Fractal Dimension

2.1.1. Precursor Type Influences the Fractal Dimension of Perovskite

Obtaining catalysts with high fractal dimension, hoping that higher fractal dimensions will lead to higher catalytic activities, is a challenging objective.

To achieve this purpose, systematic studies must be performed to analyze the relation between synthesis parameters—in every case—and catalyst fractal dimensions. From this point of view, it is a large field of research and a vast domain.

Oxides with perovskite structure of $LaCoO_3$ and $LaFeO_3$ were obtained in different preparation conditions by thermal decomposition of the precursors with maleic acid, alpha-alanine, urea and sorbitol [30,31].

Analyzing the nitrogen adsorption isotherms for lanthanum cobaltites ($LaCoO_3$) [30] and lanthanum ferrites ($LaFeO_3$) [31] obtained from different precursors, only Dubinin–Radushkevitch isotherm can be used to fit the experimental data.

The computed fractal dimension of oxide cobaltites are presented in Table 1. Results show the fractal behavior of the analyzed samples related to the BET surface; as expected, a higher fractal dimension corresponds to a higher BET surface.

Table 1. Fractal dimensions of perovskite oxides $LaCoO_3$ obtained by the direct fit of the DR isotherm; fractal dimension obtained by the Avnir–Jaroniec method; BET specific surface area (m^2/g).

Precursor	Fractal Dimension DR Isotherm	Fractal Dimension AJ Method	BET Surface (m^2/g)
Maleic acid	2.3±0.06	2.34 ± 0.06 Fractional filling 0.40–0.80	20.42
Alpha-alanine	2.62±0.06	2.62 ± 0.06 Fractional filling 0.68–0.88	32.50
Urea	2.43±0.03	2.43 ± 0.03 Fractional filling 0.45–0.82	22.62

In the case of Lanthanum ferrites, the calculation of the fractal dimension by direct fitting of the isotherm and by using the Avnir–Jaroniec method leads to low and medium values for the fractal dimension (Table 2). This indicates that J(x), the pore distribution, is not very steep, so there are more and more wide pores in the microporosity regime when the fractal dimension decreases. In this case, multilayer filling of the micropores requires higher pressure values compared to samples with larger fractal dimensions. This behavior is described by type II isotherms. Ferrites obtained using alpha-alanine or sorbitol have similar values of the fractal dimension, indicating a similar microstructure [31].

Table 2. Fractal dimensions of lanthanum ferrites ($LaFeO_3$) obtained under various preparation conditions. Reprinted from ref. [31], Copyright (2003), with permission from Elsevier.

Precursor	Fractal Dimension DR Isotherm Fitting	Fractal Dimension Avnir–Jaroniec Method
Maleic acid	2.11 ± 0.04	2.07 ± 0.01 0.4–0.6 (fractional filling range)
Alpha-alanine	2.42 ± 0.02	2.44 ± 0.05 0.46–0.93 (fractional filling range)
Urea	2.40 ± 0.02	2.49 ± 0.01 0.77–0.86 (fractional filling range)

Both Tables 1 and 2 show good concordance between the values of the fractal dimension obtained by the two methods (i.e., direct fitting by fractal adsorption isotherms and the Avnir–Jaroniec Method) and, also, that the fractal dimension value is strongly influenced by the preparation method. Larger fractal dimensions are obtained when alanine or sorbitol precursors are used.

2.1.2. The Dopant (Sr) Influences the Fractal Dimension. The Limits of Self-Similarity

Strontium-doped lanthanum cobaltites with concentrations of 0.1–0.3 have a strong effect on the fractal dimension. Our results indicate that the fractal dimension of the doped samples is larger than the fractal dimension of the pure sample (Tables 3 and 4). Good agreement between the fractal dimension computed by SEM micrographs analysis and by fitting the adsorption isotherms was found (Table 3).

Table 3. Fractal Dimension dependence on Sr concentration x for doped lanthanum cobaltites ($La_{1-x}Sr_xCoO_3$); samples were obtained by thermal decomposition of the complex precursor molar ratio La:Sr:Co:acid maleic = 1 − x:x:1:8.6. Reprinted from ref. [32], Copyright (2003), with permission from JOAM.

x	SEM Analysis	Self-Similarity Limits (nm) (SEM Analysis)	Fractal Dimension (DR Adsorption Isotherm)
0	2.32 ± 0.01	250–1110	2.34 ± 0.06
0.1	2.51 ± 0.02	100–440	2.58 ± 0.02
0.2	2.43 ± 0.01	30–330	2.48 ± 0.01

For a more accurate study, Wojsz and Terzyk [33] showed that the detailed isotherm can be fitted with a general Dubinin–Astakhov type isotherm [16], computing the limits of the micropore range as the minimum and the upper limit of the pores size at which fractal behavior is emphasized.

The same conclusions were taken from the analysis of the $La_{1-x}Sr_xCoO_3$ (x = 0–0.3) samples obtained by the thermal decomposition of alpha-alanine precursors. The results were presented in detail [34] and summarized in Table 4.

Table 4. Fractal dimension obtained by direct fitting of the nitrogen adsorption data with DR adsorption isotherms. Reprinted from ref. [34], Copyright (2018), with permission from RRC.

Sample	Fractal Dimension	Determination Coefficient
$LaCoO_3$	2.39 ± 0.03	0.987
$La_{0.9}Sr_{0.1}CoO_3$	2.45 ± 0.01	0.989
$La_{0.8}Sr_{0.2}CoO_3$	2.48 ± 0.01	0.999
$La_{0.7}Sr_{0.3}CoO_3$	2.62 ± 0.03	0.970

Extending the research on other oxide catalysts with perovskite structure such as $LaMnO_3$, both pure and doped with Sr, a different behavior was emphasized. Adding Sr into the Mn perovskite structure seems to have an inverse influence—it decreases the fractal dimension. Although the effect is not very strong, it is an unexpected observation (Table 5).

Table 5. Fractal dimensions of $La_{1-x}Sr_xMnO_3$ samples with perovskite structure. The fractal dimension was obtained by analysis of SEM micrographs and by direct fitting of the adsorption isotherms using DR fractal isotherm.

Samples	Method	Fractal Dimension	Determination Coefficient	Self-Similarity Limit (nm)
$LaMnO_3$-alanine	SEM—correlation function method	2.49 ± 0.01	0.999	100–282
		2.70 ± 0.01	0.983	282–2326
	SEM—variable scale method	2.53 ± 0.02	0.998	1000–4000
		2.74 ± 0.01	0.992	4000–12,000
	DR fractal isotherm	2.54 ± 0.04	0.972	-
$La_{0.9}Sr_{0.1}MnO_3$	SEM—correlation function method	2.20 ± 0.01	0.994	20–116
		2.62 ± 0.01	0.984	116–820
	DR fractal isotherm	2.19 ± 0.02	0.975	-
$La_{0.8}Sr_{0.2}MnO_3$	SEM—correlation function method	2.18 ± 0.01	0.996	20–136
		2.43 ± 0.01	0.988	136–700
	SEM—variable scale method	-	-	-
	DR fractal isotherm	2.20 ± 0.02	0.989	-

It can be observed that regardless of the type of catalyst ($LaCoO_3$ or $LaMnO_3$), the introduction of Sr as a dopant will reduce the self-similarity limits of the samples. This means that irrespective of whether the fractal dimension increases or decreases, the fractal properties of the catalyst manifest themselves on a smaller scaling width. The destruction of the fractal character of perovskite materials with the addition of Sr as a dopant seems to be more accentuated in the case of the $LaMnO_3$ sample than in the case of $LaCoO_3$ sample.

Our results show that there are differences between the values of the fractal dimensions obtained by the analysis of SEM micrographs and those obtained from direct fitting of the adsorption isotherms. This behavior can be explained by the fact that TEM micrographs "expose" the surface as seen by the microscope, while the adsorption isotherm "describes" the surface as "seen" by adsorbed nitrogen molecules. In other words, there will be various hidden areas in the case of TEM images not "seen" by nitrogen molecules in the case of adsorption isotherms and, thus, not counted.

To compare the results regarding the catalytic activity of perovskites, the use of the fractal dimensions calculated from the fit of the adsorption isotherms or by the Avnir–Jaroniec method is indicated. These are methods that give a more accurate description of the specific surface, which is responsible for the existence of active centers.

2.2. The Dependence of the Fractal Dimension on Catalytic Activity

Our previous results indicate that both pure and doped $LaCoO_3$ samples [34] exhibit catalytic activity in the hydrogen peroxide decomposition reaction following the sequence $LaCoO_3$ < $La_{0.9}Sr_{0.1}CoO_3$ < $La_{0.8}Sr_{0.2}CoO_3$ < $La_{0.7}Sr_{0.3}CoO_3$. Therefore, as the fractal dimension increases, the catalytic activity also increases (Table 4). This correlation can be explained by the increase in catalytic activity due to the number of vacancies generated by partial substitution of La by the Sr ions. [35,36].

At the same time, there is a linear dependence of the logarithm of the pre-exponential factor *ln*A and the apparent activation energy for the hydrogen peroxide decomposition reaction, indicating a compensation effect (Figure 1). This effect can be explained by the existence of a non-uniform energetic surface and/or by the dependence of the active centers number on the presence of the Sr ions on the catalyst surface.

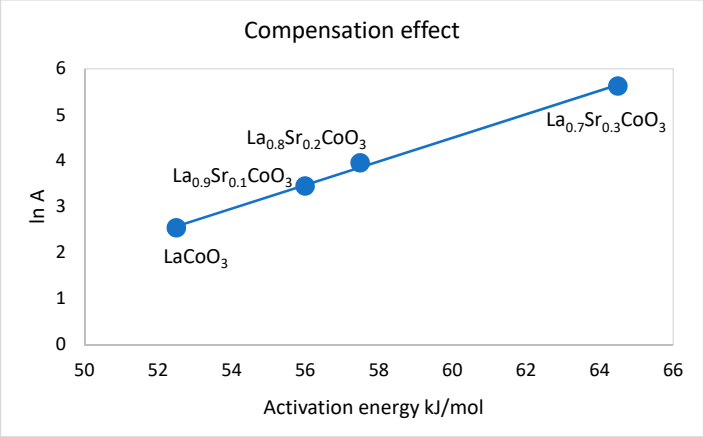

Figure 1. Compensation effect in the H_2O_2 decomposition reaction. Reprinted from ref. [34], Copyright (2018), with permission from RRC.

Trypolskyi and al. [37] showed that the activation energy in catalytic processes depends on the fractal surface dimension. Our results emphasize the same behavior as the reported paper (Figures 2 and 3).

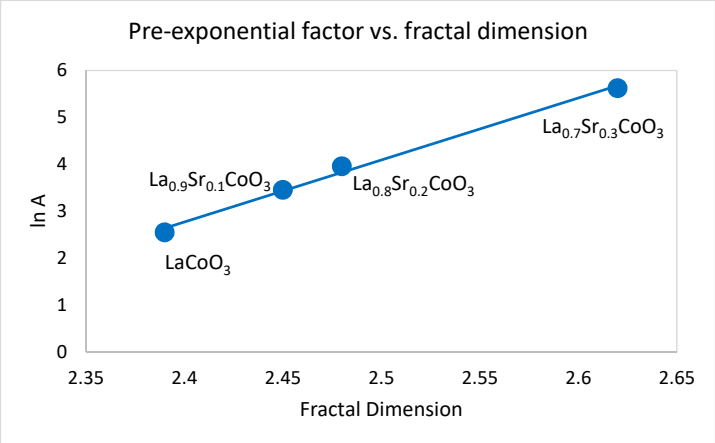

Figure 2. Pre-exponential factor vs. fractal dimension. Reprinted from ref. [34], Copyright (2018), with permission from RRC.

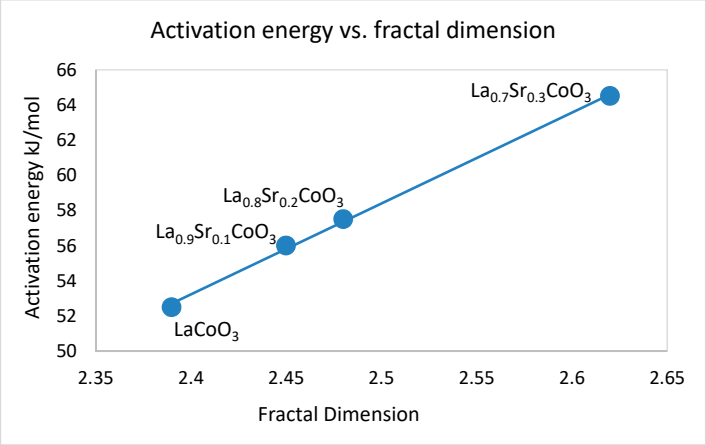

Figure 3. Activation energy versus fractal dimension. Reprinted from ref. [34], Copyright (2018), with permission from RRC.

Sr-doped $LaMnO_3$ catalyst with various concentrations (x = 0–0.2) were also investigated in the methane combustion reaction (Figure 4).

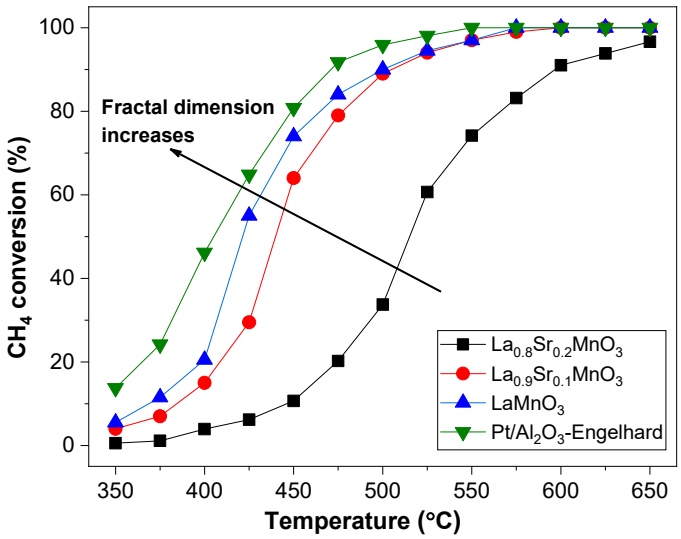

Figure 4. The catalytic activity for methane combustion.

It is observed that the conversion of methane vs. temperature in the total oxidation of methane depends on the used catalyst. Better results were obtained for the pure catalyst compared to those doped with strontium cation. For comparison, the results obtained using Pt/Al_2O_3 1 wt.% commercial catalyst (Engelhard) are also presented. The reactivity of the three samples decreases following the sequence $La_{0.8}Sr_{0.2}MnO_3$ < $La_{0.9}Sr_{0.1}MnO_3$ < $LaMnO_3$. This is in good agreement with the decrease of the computed fractal dimension according to the same sequence. Moreover, the activation energy of the methane oxidation reaction decreases with the decreases of fractal dimension (Figure 5).

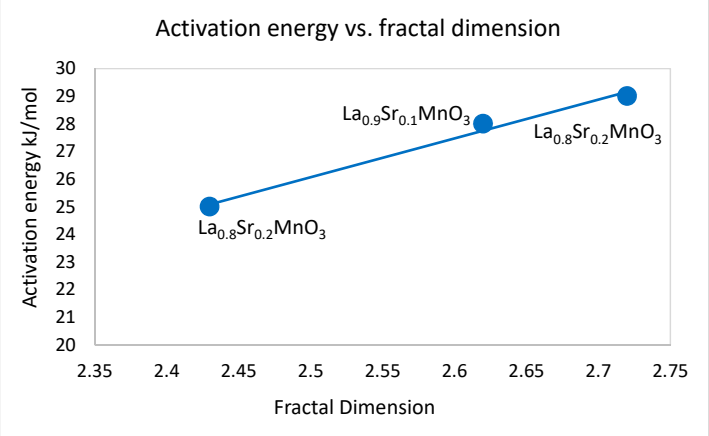

Figure 5. The dependence of the activation energy on the fractal dimension in the methane oxidation reaction when perovskite catalysts of the $La_{1-x}Sr_xMnO_3$ type are used.

2.3. The Fractal Structure of Mono- and Bi-Metallic Nanoparticles

Mono- and bi-metallic nanoparticles of Pd, Pd-Cu and Pd-Ag were obtained under different conditions, as is described in detail in [38]. Fractal behavior was investigated by TEM micrographs analysis. The D_0 fractal dimensions and the lacunarities [20] of the nanoparticles were computed using the "box counting" method and the modified black and white TEM images, considering nanoparticles as 2D black disks (Tables 6 and 7).

Table 6. The «box-counting » fractal dimension and the lacunarity of monometallic and alloy nanoparticles. Reprinted from ref. [38], Copyright (2018), with permission from Elsevier.

Sample	Fractal Dimension D_0	Lacunarity A_0
Pd	1.427 ± 0.457	8.39×10^4
Pd-Cu 4:1 Alloy	1.912 ± 0.014	8.24×10^5
Pd-Cu 1:1 Alloy	1.681 ± 0.015	2.57×10^5
Pd-Cu 1:4 Alloy	1.799 ± 0.035	2.36×10^5

Table 7. The "box-counting" fractal dimensions D_0, and the fractal dimensions D (λ_m), D (λ_1) and D (λ_2) obtained by gray level analysis, where D (λ_1) and D (λ_2) are the fractal dimensions characteristic for the nucleation processes, the "core" fractal dimension and the "shell" fractal dimension. Meanwhile, D (λ_m) is the fractal dimension of the whole structure. Reprinted from ref. [38], Copyright (2018), with permission from Elsevier.

Sample	D_0	λ_m	D (λ_m)	λ_1	D (λ_1)	λ_2	D (λ_2)
Pd-Cu Core-shell	1.841 ± 0.009	140	1.773 ± 0.048	170	1.632 ± 0.074	130	1.826 ± 0.037
Cu-Pd Inverse core-shell	1.855 ± 0.010	110	1.796 ± 0.026	130	1.827 ± 0.029	100	1.813 ± 0.010
Pd-Ag Core-shell	1.854 ± 0.018	130	1.819 ± 0.107	160	1.669 ± 0.061	120	1.863 ± 0.079
Ag-Pd Inverse Core-shell	1.875 ± 0.032	100	1.836 ± 0.023	110	1.776 ± 0.018	90	1.884 ± 0.021

The results presented in (Tables 6 and 7) indicate self-similarity and fractal properties for all the studied catalysts. It should be noted that the grey-level fractal analysis of TEM images leads to the identification of the structure of nanoparticles (alloy or core-shell type), obtaining the fractal dimension both for the core and for the shell [38].

Another bimetallic nanoparticle system characterized by fractal properties is Pt-Cu prepared in two synthesis variants: with low molar ratio of PVP/Pt^{4+} = 5 $(Pt\text{-}Cu)_L$, and high molar ratio (Pt-Cu)s, PVP/Pt^{4+} = 10, respectively, as described in the literature [39]. Fractal properties are summarized in (Table 8).

Table 8. Results of the fractal analysis performed on Pt-Cu nanoparticles. Reprinted from ref. [39], Copyright (2015), with permission from RSC.

Sample	Calculation Method	Fractal Dimension	Correlation Coefficient	Self-Similarity Domain/nm
$(Pt\text{-}Cu)_L$	Correlation function	2.50 ± 0.01 2.70 ± 0.01	0.991 0.981	1.4–2.5 2.5–5.0
	Variable length scale	2.68 ± 0.01	0.984	5.0–27.5
$(Pt\text{-}Cu)_S$	Correlation function	2.40 ± 0.01 2.73 ± 0.01	0.998 0.996	1.4–2.2 7.5–12.5
	Variable length scale	2.88 ± 0.01	0.992	12.5–22.5

As was described in detail in article [39], the PVP/Pt^{4+} low molar ratio leads to the formation of larger nanoparticles (between 2 nm and 5 nm), while a PVP/Pt^{4+} high molar ratio leads to nanoparticles of diameters between 1 nm and 2 nm. This observation can be seen in Table 8 from the analysis of self-similarity limits. The fractal behavior of $(Pt\text{-}Cu)_L$ nanoparticles indicates a mixture of small particles 1.4 nm–2.5 nm and, respectively, large 2.5 nm–5 nm ones, between which there are long-distance correlations characterized by a fractal size of 2.68. On the other hand, $(Pt\text{-}Cu)_s$ sample has an homogeneous structure composed of particles of 1.4 nm–2.2 nm, with medium and long-correlated fractal dimensions of 2.73 and 2.88, respectively.

One of the conclusions of the cited article is that unsupported $(Pt\text{-}Cu)_s$ nanoparticles have a much better catalytic performance than $(Pt\text{-}Cu)_L$ nanoparticles in terms of the catalytic reduction of NO_3^- ions. Beyond the explanations provided in detail by the cited article, it is observed that catalytic performance can be correlated with long-distance fractal dimension: the larger fractal dimension $(Pt\text{-}Cu)_s$ nanoparticles, D = 2.88, will favor catalytic activity compared to the lower fractal dimension $(Pt\text{-}Cu)_L$ nanoparticles, D = 2.68.

The catalytic applications of bimetallic nanoparticles are diverse: oxidative conversion of methane [40], oxidation of CO [41], reduction of nitrates [42], oxidation of methanol [43], etc. In most cases, bimetallic nanoparticles have shown better catalytic activity than their constituent metals.

We will further refer to alumina supported Pt-Cu nanoparticles studied in the context of total oxidation of methane. The catalytic behavior of the above mentioned nanoparticles was compared with an available catalyst Pt/Al_2O_3 1 wt.% (Engelhard) with the same metal loading level (1wt. %) (Figure 6) [44].

Fractal analysis of TEM images (images for which the background was removed in order to improve image quality) shows a bimodal fractal behavior characterized by two fractal dimensions: one for low scales and another for large scales. The inflection point (contact between the two self-similarity domains) is located at 1.2 nm and it is an indication of the average radius of Pt-Cu particles. For wide scaling domains (greater than 4.5 nm) the structure does not show fractal behavior (Table 9).

Table 9. The fractal dimension of $Pt\text{-}Cu/Al_2O_3$ obtained using the correlation function method. Reprinted from ref. [44], Copyright (2011), with permission from Elsevier.

Fractal Dimension	Linear Correlation Coefficient	Self-Similarity Domain
2.39 ± 0.01	0.996	0.18–1.24
2.81 ± 0.01	0.975	1.24–4.50

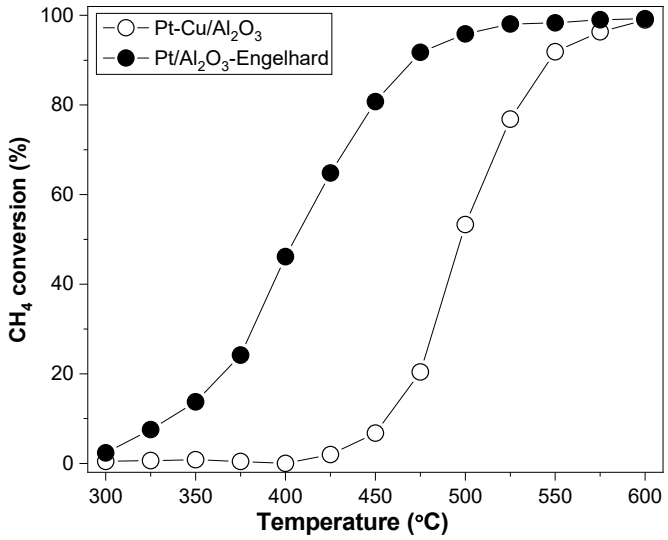

Figure 6. Methane conversion versus temperature using two different catalysts: Pt-Cu/Al_2O_3 and Pt/Al_2O_3. Reprinted from ref. [44], Copyright (2011), with permission from Elsevier.

Although, the fractal size of the Pt-Cu/Al_2O_3 bimetallic system is quite large on a wide scale (2.81) compared to a commercial Pt/Al_2O_3 catalyst, from the obtained experimental results we observed that there is a decrease in the catalytic activity; an explanation lies in the nanoparticles' surface chemical composition due to copper enrichment.

2.4. The Influence of the Fractal Dimension of Supported Nanoparticles on Surface Basicity

In order to deepen how fractal character influences the physico-chemical properties of the catalysts, we further analyze a series of Rh nanoparticles on various supports: Al_2O_3, TiO_2 and WO_3 [45].

The studied based-nanoparticle catalysts Rh/Al_2O_3, Rh/TiO_2, Rh/WO_3 showed fractal behavior (Tables 10 and 11), both before and after CO_2-TPD experiments, on a wide self-similarity domain. There is a strong correlation between the fractal dimension and the basicity of the studied catalysts.

Table 10. Fractal dimensions before CO_2-TPD from the analysis of TEM micrographs, using two methods: "C" meaning the correlation function method, and "S" the variable length scale method [45].

Sample	Fractal Dimension	Correlation Coefficient	Self-Similarity Domain (nm)
Rh/Al_2O_3	2.872 ± 0.001 (C) 2.784 ± 0.051 (S)	0.9910 0.8186	4.4–14.4 7.2–11.8
Al_2O_3	2.952 ± 0.001 (C) 2.962 ± 0.004 (S)	0.9375 0.9549	0.7–8.1 1.4–2.8
Rh/TiO_2	2.733 ± 0.001 (C) 2.832 ± 0.009 (S)	0.9884 0.9649	4.9–14.4 5.4–17.3
TiO_2	2.831 ± 0.001 (C) 2.911 ± 0.017 (S)	0.857 0.925	6.5–11 2.4–3.00
Rh/WO_3	2.490 ± 0.001 (C) 2.330 ± 0.001 (C) 2.469 ± 0.035 (S) 2.226 ± 0.047 (S)	0.9975 0.9991 0.9747 0.9334	0.2–2.7 2.7–13.8 4.5–11 11–29.3
WO_3	2.660 ± 0.004 (C) 2.293 ± 0.002 (C) 2.652 ± 0.042 (S)	0.990 0.986 0.949	0.2–1.2 1.8–5.0 4.1–5.9

Table 11. Fractal dimensions (before and after CO_2-TPD) obtained by direct fitting of adsorption data with DR adsorption isotherms [45].

Sample	Fractal Dimension	Correlation Coefficient	Self-Similarity Domain (p/p_0)	CO_2-TPD
Rh/Al_2O_3	2.607 ± 0.004	0.9986	0.033–0.850	Before
	2.534 ± 0.009	0.9973	0.011–0.350	After
	2.623 ± 0.002	0.9998	0.350–0.800	After
Rh/TiO_2	2.604 ± 0.003	0.9989	0.011–0.750	Before
	2.292 ± 0.011	0.9980	0.005–0.350	After
	2.548 ± 0.005	0.9987	0.350–0.850	After
Rh/WO_3	2.448 ± 0.012	0.9977	0.005–0.200	Before
	2.589 ± 0.014	0.9889	0.200–0.750	Before
	2.595 ± 0.008	0.9970	0.005–0.350	After
	2.003 ± 0.003	0.9993	0.350–0.875	After

Results showed (Tables 10 and 11) that adding Rh nanoparticles on the corresponding supports leads to a decrease in the fractal dimension of the Rh/support system, compared to the fractal dimension of the support itself. This decrease in fractal dimension can be explained by blocking the surface pores on the support and/or by encapsulating Rh via strong metal support-interaction (SMSI) [28]. The bimodal character of the WO_3 substrate is preserved even when Rh nanoparticles are added. The fractal dimensions obtained by fitting the adsorption isotherms with the DR isotherms (in the capillary condensation regime) are smaller than the fractal dimensions obtained by the image analysis of the TEM micrographs for Rh/Al_2O_3 and Rh/TiO_2 samples. This behavior can be explained by the fact that fractal dimension obtained from the analysis of the adsorption isotherm is an expression of the pore filling capacity on the surface of the adsorbate, while the fractal dimension obtained from the TEM image analysis measures correlations and similarities of all points (visible in TEM) on the studied surface. The last sample (Rh/WO_3) has the same bimodal characteristic, both in terms of the DR fractal dimension and in terms of the TEM fractal dimension.

Figures 7–10 present the number of basic centers dependence on the fractal dimension of the system/support.

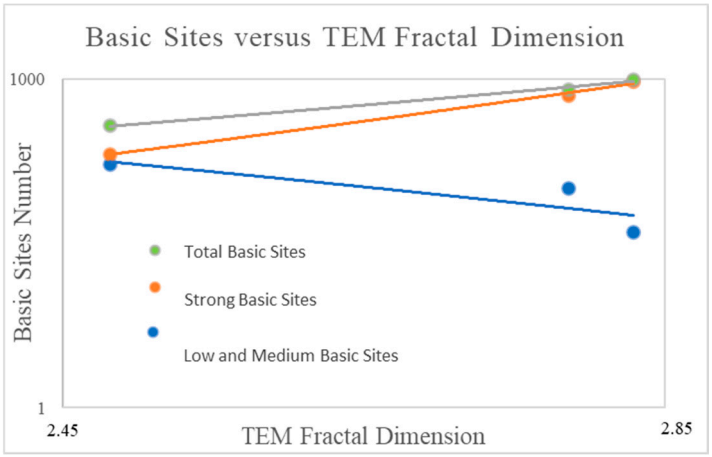

Figure 7. Basic sites: total basic sites, strong basic sites and low and medium basic sites dependencies on TEM fractal dimension of NP/support (double-logarithmic scale).

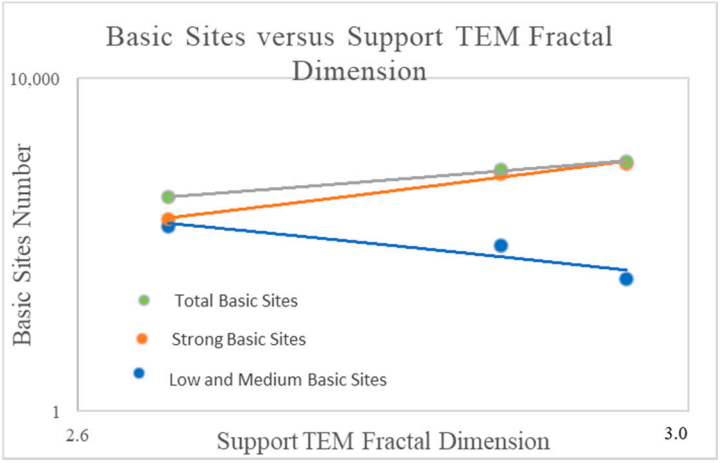

Figure 8. Basic sites: total basic sites, strong basic sites and low and medium basic sites dependencies on TEM fractal dimension of the support (double-logarithmic scale).

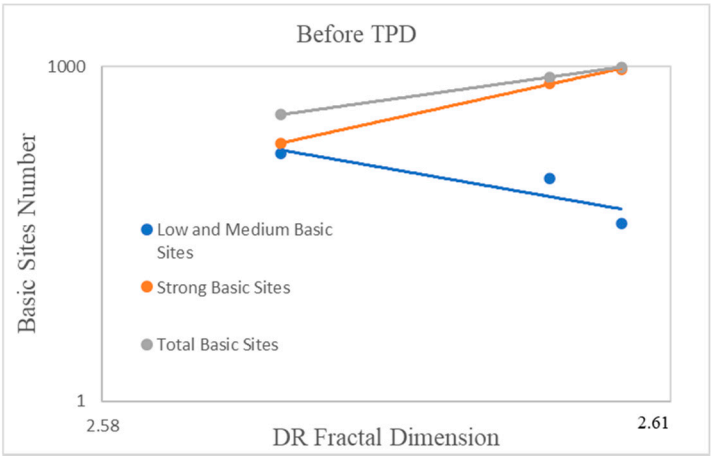

Figure 9. Basic sites versus DR Fractal Dimension before CO_2-TPD (double-logarithmic scale).

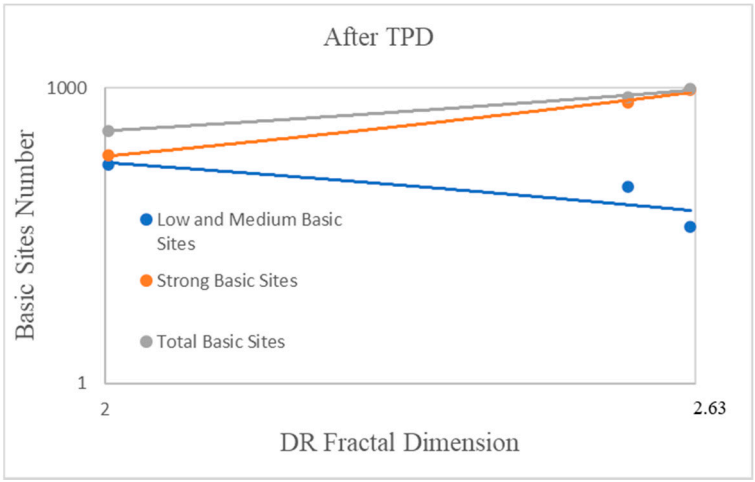

Figure 10. Basic sites vs. DR Fractal Dimension after CO_2-TPD measurements (double-logarithmic scale).

It is observed that the number of low and medium basic centers decreases slightly with the TEM fractal dimension of the supported nanoparticles, but also with the TEM

fractal dimension of the support. On the other hand, the total number of strong basic centers increases with the same fractal dimensions. The same behavior is observed in the case of the fractal dimension obtained by analyzing the adsorption isotherm, both before and after CO_2-TPD. This behavior leads to the idea that large fractal dimensions favor strong basic centers, while small fractal dimensions favor weak basic centers.

A system with a large fractal dimension will favor the strong metal support-interaction (SMSI) leading to the formation of monodentate carbonate (Rh/Al_2O_3 and Rh/TiO_2) and implicitly of the strong basic centers. Weak and medium centers, usually attributed to the HO group, forming bicarbonate species with CO_2 or bidentate carbonate, are favored by surfaces with fewer defects, pores, fewer irregularities and lower fractal dimension.

In order to improve the DRM (Dry Reforming of Methane), catalytic activity of Rh/Al_2O_3, Rh/TiO2 and Rh/WO_3 and a large number of active centers are needed [46,47]. One way to achieve this is to use supports with a large fractal dimension; supports that will lead to NP systems/supports with a large fractal dimension and, therefore, to a large number of basic centers.

3. Discussion Regarding the Fractal Properties of Catalysts

The novelty element of this study is its correlation of the fractal behavior (fractal dimension) of catalysts with their catalytic activity as well as their specific chemical properties. We started from the general observation that a "perfect" catalyst should have an "ideal" fractal structure [12]. This idea involves structures of catalysts with very large specific surfaces and therefore many active centers capable of favoring chemical reactions. In reality, catalysts cannot be ideal mathematical fractals. No real structure can be described as an ideal mathematical fractal. It would require that it could be characterized by an infinite field of self-similarity and a deterministic self-similar structure. In the real world, systems are characterized by fractal properties only on restricted domains of self-similarity, which is always of necessary mention in the characterization of systems. Obviously, if we study a phenomenon on the order of nanometers, we are interested in self-similarity properties at this scale and not at scale lengths on the order of meters.

Self-similarity domains, especially the intersection areas of the domains with different fractal dimensions, give information regarding particle size, bi-modality of the sample, etc.

One of the methods used in determining fractal size is the direct fitting of the adsorption data with DR adsorption isotherms. The usual way to construct DR fractal isotherms is to consider the object as a fractal pore system. However, are real catalysts actually real fractal pore systems? In addition, if they are not, can we talk about their fractal dimension? Alternatively, can fractal adsorption isotherms, which are based on the idea of a pore fractal system [16], be used to determine the fractal dimension?

There are studies [48] showing that an optimal catalyst cannot be described as a fractal pore system realistically, though the fractal dimension could be an indication of the roughness of the analyzed samples.

Rudzinschi and. al. [49] show that fractal adsorption isotherms can be deduced without assuming the existence of a fractal pore system. The actual nature of the partially correlated solid surfaces is sufficient to deduce the fractal isotherms used. Surface energy heterogeneities in relation to fractal geometric non-uniformities lead to the deduction of the Dubinin–Radushkevitch isotherm without resorting to the questionable fractal distribution of pores [49]. In conclusion, the fractal dimension calculated by direct fitting of the adsorption isotherms with the DR equation reflects a real characteristic of self-similarity of the catalysts and is not a mathematical artefact.

4. Materials and Methods

4.1. Synthesis of Materials

Mixed perovskite-type oxides (cobaltite and ferrite) were prepared by calcination in air of isolated complex precursors (urea-base precursor, alpha-alanine-base precursor, sorbitol-

base precursor, acid maleic-base precursor). Details on catalyst synthesis are presented in extenso in [30–32,34,50,51].

Bimetallic nanoparticle samples were prepared using the alkaline polyol method, an easy and versatile synthesis method described in detail in the literature [38,39,44,45,52].

4.2. Methods

4.2.1. Fractal Dimension Determination Using Image Analysis

The mathematical determination of the fractal dimension has its basis in the fundamental fractal property of self-similarity [2]. Self-similarity is the property of an object to appear the same when seen from near or far. The mathematical description of this property is given by the following formula:

$$N(r/R) \sim (r/R)^{-D} \quad (1)$$

where D is the fractal dimension, N(r/R) is the number of r size boxes that can cover an object of size R.

Starting from this definition and from its mathematical expression, various methods for determining both the fractal dimension and the scaling domain can be imagined, i.e., the values for r for which Equation (1) is valid.

SEM, TEM and AFM micrographs can be analyzed using various methods, such as the Fourier transform method [53], the box-counting method [2], the mass-radius dependence method [54], the correlation function method [53,55] and the variable scaling method [56].

4.2.2. Fractal Dimension Determination Using Adsorption Isotherms

The fractal size of the catalysts can be determined by adsorption experiments, either by direct fitting the adsorption isotherms or by the Avnir–Jaroniec method. Experimental adsorption isotherms have been shown to be efficiently fitted with the Dubinin–Radushkevitch isotherm [16]:

$$\theta = K[\ln(p_o/p)]^{D-3} \quad (2)$$

where θ is the relative adsorption, K is a characteristic constant, p_0 and p are saturation and equilibrium pressures and D is the fractal dimension.

Other isotherms (such as those presented below—Equations (3) and (4)) did not lead to viable results regarding the fractal dimension.

- the BET fractal isotherm obtained by Fripiat [57]:

$$\theta = N/N_m = \frac{c}{1+(c-1)x} \sum_{n=1}^{\infty} n^{2-D} x^n \quad (3)$$

- the Frenkel-Halsey-Hill [58] isotherm:

$$N/N_m = (z/a)^{3-D} = [\gamma/(-\ln x)]^{(3-D)/3}$$
$$\gamma \equiv \alpha/(kTa^3),\ 2 \le D < 3, \quad (4)$$
$$x \equiv P/P_o, z = [\alpha/(kT\ln(P_o/P))]^{1/3}$$

where N_m, is the monolayer volume, a is the monolayer thickness and α is the difference of the interaction constants.

It is noteworthy that although the Frenkel–Halsey–Hill isotherm shape resembles the Dubinin–Radushkevitch fractal isotherm, the exponent is different for the two isotherms. The use of the Frenkel–Halsey–Hill isotherm can lead, in some cases, to values of fractal size of over 4, which is obviously unrealistic.

4.2.3. Avnir–Jaroniec Method

This method is described in detail in the literature [24]. It is based on the micropores volume calculation and, thus, the dependence of the fractional filling on pressure is computed, leading to the local determination of the Avnir–Jaroniec fractal dimension. The zone where the fractal dimension is constant gives the value of the fractal dimension, but also the domain of self-similarity.

5. Conclusions

The present paper depicted some catalysts that have been shown to have fractal properties, with a large domain of self-similarity.

The experimental results revealed that the synthesis method of catalysts influences the fractal dimension. Both the nature of the precursor as well as the introduction of dopants changes the fractal dimension for mixed oxide perovskite-type catalysts. Moreover, fractal analysis was used to obtain information regarding the morphology/geometry of the samples.

The fractal dimension is, as well, an indicator of the number of basic centers on the surface of the supported nanoparticles studied, basic centers that are directly related to the catalytic activity of these catalysts.

Moreover, very importantly, both catalytic activity in various reactions and the activation energy strongly depend on the fractal dimension of the catalysts. Catalytic activity is undoubtedly favored by catalysts with large fractal dimensions.

Author Contributions: Conceptualization, G.D. and F.P.; methodology, G.D.; investigation, D.B., F.P., R.S. and M.R.; data curation, I.B. and F.P.; writing—original draft preparation, G.D. and N.I.I.; writing—review and editing, G.D. and F.P.; supervision, I.B. and N.I.I.; funding acquisition, F.P. All authors have read and agreed to the published version of the manuscript.

Funding: This research was funded by Unitatea Executiva pentru Finantarea Invatamantului Superior, a Cercetarii, Dezvoltarii si Inovarii (UEFISCDI), grant number PN III—26PTE/2020 DENOX.

Conflicts of Interest: The authors declare no conflict of interest.

References

1. Mandelbrot, B.B. *Fractals: Form, Chance and Dimension*; Freeman, W.H., Ed.; MANDELBROT. WH Freeman and Co.: San Francisco, CA, USA, 1977.
2. Mandelbrot, B.B. *The Fractal Geometry of Nature*; Freeman, W.H., Ed.; MANDELBROT. WH Freeman and Co.: San Francisco, CA, USA, 1982.
3. Sorensen, C.M. Light scattering by fractal aggregates: A review. *Aerosol Sci. Technol.* **2001**, *35*, 648–687. [CrossRef]
4. Abed, A.T.; Abu-AlShaer, M.J.; Jawad, A.M. Fractal antennas for wireless communications. In *Modern Printed-Circuit Antennas*; Al-Rizzo, H., Ed.; IntechOpen: London, UK, 2020.
5. Witten, T.A.; Sander, L.M. Diffusion-limited aggregation. *Phys. Rev. B* **1983**, *27*, 5686–5697. [CrossRef]
6. Zhou, H.W.; Xie, H. Direct estimation of the fractal dimensions of a fracture surface of rock. *Surf. Rev. Lett.* **2003**, *10*, 751–762. [CrossRef]
7. Kopelman, R. Fractal Reaction Kinetics. *Science* **1988**, *241*, 1620–1626. [CrossRef] [PubMed]
8. Mattfeldt, H.W.; Gottfried, H.W.; Schmidt, V.; Kestler, H.A. Classification of spatial textures in benign and cancerous glandular tissues by stereology and stochastic geometry using artificial neural networks. *J. Microsc.* **1999**, *198*, 143–158.
9. Socoteanu, R.; Anastasescu, M.; Dobrescu, G.; Boscencu, R.; Vasiliu, G.; Constantin, C. AFM imaging, fractal analysis and in vitro cytotoxicity evaluation of Zn (II) vs. Cu (II) porphyrins. *Chaos Solit. Fractals* **2015**, *77*, 304–309. [CrossRef]
10. Hang, J.T.; Kang, Y.; Xu, G.-K.; Gao, H. A hierarchical cellular structural model to unravel the universal power-law rheological behavior of living cells. *Nat. Commun.* **2021**, *12*, 6067. [CrossRef] [PubMed]
11. Avnir, D.; Farin, D.; Pfeifer, P. Surface geometric irregularity of particulate materials: The fractal approach. *J. Colloid Interface Sci.* **1985**, *103*, 112–123. [CrossRef]
12. Rothschild, W.G. Fractals in heterogeneous catalysis. *Catal. Rev. Sci. Eng.* **1991**, *33*, 71–107. [CrossRef]
13. Pfeifer, P.; Obert, M.; Cole, M.W. Fractal BET and FHH theories of adsorption: A comparative study. *Proc. R. Soc. Lond. A* **1989**, *423*, 169–188.
14. Pfeifer, P.; Avnir, D.; Farin, D. *Complex Surface Geometry in Nano-Structure Solids: Fractal Versus Bernal-Type Models. Large Scale Molecular Systems—Quantum and Stochastic Aspects*; NATO ASI, Series B; Gans, W., Blumen, A., Amann, A., Eds.; Plenum: New York, NY, USA, 1991; pp. 215–229.

15. Meakin, P. Fractals and Reactions on Fractals. In *Reactions in Compartmentalized Liquids*; Knoche, W., Schomäcker, R., Eds.; Springer: Berlin/Heidelberg, Germany, 1989; pp. 173–198.
16. Avnir, D.; Jaroniec, M. An isotherm equation for adsorption on fractal surfaces of heterogeneous porous materials. *Langmuir* **1989**, *5*, 1431–1433. [CrossRef]
17. Pfeifer, P.; Kenntner, J.; Cole, M.W. Detecting capillary condensation in the absence of adsorption/desorption hysteresis. In *Fundamentals of Adsorption*; American Institute of Chemical Engineers: New York, NY, USA, 1991; pp. 689–700.
18. Ludlow, D.K.; Moberg, T.P. Technique for determination of surface fractal dimension using a dynamic flow adsorption instrument. *Instrum. Sci. Technol.* **1990**, *19*, 113–123. [CrossRef]
19. Farin, D.; Avnir, D.; Pfeifer, P. Fractal dimensions of surfaces. The use of adsorption data for the quantitative evaluation of geometric irregularity. *Particul. Sci. Technol.* **1984**, *2*, 27–35. [CrossRef]
20. Pfeifer, P.; Stella, A.L.; Toigo, F.; Cole, M.W. Scaling of the dynamic structure factor of an adsorbate on a fractal surface. *Europhys. Lett.* **1987**, *3*, 717–722. [CrossRef]
21. Cheng, E.; Cole, M.W.; Pfeifer, P. Defractalization of films adsorbed on fractal surfaces. *Phys. Rev. B* **1989**, *39*, 12962–12965. [CrossRef]
22. Avnir, D.; Farin, D. Fractal scaling laws in heterogeneous chemistry: Part I: Adsorptions, chemisorptions and interactions between adsorbates. *N. J. Chem.* **1990**, *14*, 197–206.
23. Pfeifer, P.; Johnston, G.P.; Deshpande, R.; Smith, D.M.; Hurd, A.J. Structure analysis of porous solids from preadsorbed films. *Langmuir* **1991**, *7*, 2833–2843. [CrossRef]
24. Kaneko, K.; Sato, M.; Suzuki, T.; Fujiwara, Y.; Nishikawa, K.; Jaroniec, M. Surface fractal dimension of microporous carbon fibres by nitrogen adsorption. *J. Chem. Soc. Faraday Trans.* **1991**, *87*, 179–184. [CrossRef]
25. Gutfraind, R.; Sheintuch, M.; Avnir, D. Fractal and multifractal analysis of the sensitivity of catalytic reactions to catalyst structure. *J. Chem. Phys.* **1991**, *95*, 6100–6111. [CrossRef]
26. Sanders, L.M.; Ghaisas, S.V. Fractals and patterns in catalysis. *Phys. A* **1996**, *233*, 629–639. [CrossRef]
27. Che, M.; Bennett, C.O. The influence of particle size on the catalytic properties of supported metals. *Adv. Catal.* **1989**, *36*, 55–172.
28. Matsubu, J.; Zhang, S.; DeRita, L.; Marinkovic, N.S.; Chen, J.G.; Graham, G.W.; Pan, X.; Christopher, P. Adsorbate-mediated strong metal–support interactions in oxide-supported Rh catalysts. *Nat. Chem.* **2017**, *9*, 120–127.
29. Huang, R.; Wu, J.; Zhang, M.; Liu, B.; Zheng, Z.; Luo, D. Strategies to enhance photocatalytic activity of graphite carbon nitride-based photocatalysts. *Mater. Des.* **2021**, *210*, 110040.
30. Dobrescu, G.; Berger, D.; Papa, F.; Fangli, I.; Rusu, M. Fractal dimensions of lanthanum cobaltites samples by adsorption isotherm method. In *Interdisciplinary Applications of Fractal and Chaos Theory*; Dobrescu, R., Vasilescu, C., Eds.; Editura Academiei Romane: Bucuresti, Romania, 2004; pp. 295–302.
31. Dobrescu, G.; Berger, D.; Papa, F.; Ionescu, N.I. Fractal dimension of lanthanum ferrite samples by adsorption isotherm method. *Appl. Surf. Sci.* **2003**, *220*, 154–158. [CrossRef]
32. Dobrescu, G.; Berger, D.; Papa, F.; Ionescu, N.I.; Rusu, M. Fractal analysis of micrographs and adsorption isotherms of $La_{1-x}Sr_xCoO_3$ samples. *J. Optoelectron. Adv.* **2003**, *5*, 1433–1437.
33. Wojsk, R.; Terzyk, A.P. The structural parameters of microporous solid, including fractal dimension, on the basis of the potential theory of adsorption-the general solution. *Comput. Chem.* **1997**, *21*, 83–87.
34. Papa, F.; Berger, D.; Dobrescu, G.; State, R.; Ionescu, N.I. Correlation of the Sr-dopant content in $La_{1-x}Sr_xCoO_3$ with catalytic activity for hydrogen peroxide decomposition. *Rev. Roum. Chim.* **2018**, *63*, 447–453.
35. Aoa, M.; Pharma, G.H.; Sage, V.; Pareeka, V. Structure and activity of strontium substituted $LaCoO_3$ perovskite catalysts forsyngas conversion. *J. Mol. Catal. A Chem.* **2016**, *416*, 96–104. [CrossRef]
36. Prasad, D.H.; Park, S.Y.; Oh, E.O.; Ji, H.; Kim, H.R.; Yoon, K.J.; Yoon, J.; Son, J.W.; Lee, J.H. Synthesis of nano-crystalline $La_{1-x}Sr_xCoO_{3-\delta}$ perovskite oxides by EDTA-citrate complexing process and its catalytic activity for soot oxidation. *Appl. Catal. A Gen.* **2012**, *447*, 100–106. [CrossRef]
37. Trypolskyi, A.I.; Gurnyk, T.M.; Strizhak, P.E. Fractal dimension of zirconia nanopowders and their activity in the CO oxidation. *Catal. Commun.* **2011**, *12*, 766–771. [CrossRef]
38. Dobrescu, G.; Papa, F.; State, R.; Balint, I. Characterization of bimetallic nanoparticles by fractal analysis. *Powder Technol.* **2018**, *338*, 905–914. [CrossRef]
39. Miyazaki, A.; Matsuda, K.; Papa, F.; Scurtu, M.; Negrila, C.; Dobrescu, G.; Balint, I. Impact of particle size and metal-support interaction on denitration behavior of wee-defined Pt-Cu nanoparticles. *Catal. Sci. Technol.* **2015**, *5*, 492–503. [CrossRef]
40. Lanza, R.; Canu, P.; Jaras, S.G. Partial oxidation of methane over Pt-Ru bimetallic catalyst for syngas production. *Appl. Catal. A Gen.* **2008**, *348*, 221–228. [CrossRef]
41. Liao, P.C.; Carberry, J.J.; Fleisch, T.H.; Wolf, E.E. CO oxidation activity and XPS studies of $PtCu_\gamma$-Al_2O_3 bimetallic catalysts. *J. Catal.* **1982**, *74*, 307–316. [CrossRef]
42. Soares, O.S.G.P.; Órfão, J.J.M.; Pereira, M.F.R. Bimetallic catalysts supported on activated carbon for the nitrate reduction in water: Optimization of catalysts composition. *Appl. Catal. B Environ.* **2009**, *91*, 441–448. [CrossRef]
43. Baglio, V.; Stassi, A.; Di Blasi, A.; D'Urso, C.; Antonucci, V.; Arico, A.S. Investigation of bimetallic Pt-M/C as DMFC cathode catalysts. *Electrochim. Acta* **2007**, *53*, 1360. [CrossRef]

44. Papa, F.; Negrila, C.; Dobrescu, G.; Miyazaki, A.; Balint, I. Preparation, characterization and catalytic behavior of Pt-Cu nanoparticles in methane combustion. *J. Nat. Gas Chem.* **2011**, *20*, 537–542. [CrossRef]
45. Dobrescu, G.; Papa, F.; Atkinson, I.; Culita, D.; Balint, I. Correlation between the basicity and the fractal dimension of Rh-nanoparticles supported on Al_2O_3, TiO_2 and WO_3. *IOSR-JAC* **2021**, *14*, 11–25.
46. Jang, W.; Shim, J.; Kim, H.; Yoo, S.; Roh, H. A review on dry reforming of methane in aspect of catalytic properties. *Catal. Today* **2019**, *324*, 15–26. [CrossRef]
47. Wang, H.Y.; Ruckenstein, E. Carbon dioxide reforming of methane to synthesis gas over supported rhodium catalysts: The effect of support. *Appl. Catal. A Gen.* **2000**, *204*, 143–152. [CrossRef]
48. Curtis Conner, W.; Bennett, C.O. Are the pore and surface morphologies of real fractal catalysts? *J. Chem. Soc. Faraday Trans.* **1993**, *89*, 4109–4114. [CrossRef]
49. Rudzinski, W.; Lee, S.L.; Sanders yan, C.C.; Panczyk, T. A fractal approach to adsorption on heterogeneous solid surfaces. 1. The relationship between geometric and energetic surface heterogeneities. *J. Phys. Chem. B* **2001**, *105*, 10847–10856. [CrossRef]
50. Berger, D.; Matei, C.; Papa, F.; Voicu, G.; Fruth, V. Pure and doped $_{LaCoO3}$ obtained by combustion method. *Prog. Solid State Chem.* **2007**, *35*, 183–191. [CrossRef]
51. Dobrescu, G.; Berger, D.; Papa, F.; Fangli, I.; Sitaru, I. Fractal analysis of micrographs and adsorption isotherms of $LaCoO_3$ and $LaFeO_3$ samples. *Ann. West Univ. Timis. Ser. Chem.* **2003**, *12*, 1505–1512.
52. Papa, F.; Negrila, C.; Miyazaki, A.; Balint, I. Morphology and chemical state of PVP-protected Pt, Pt-Cu and Pt-Ag nanoparticles prepared by alkaline polyol method. *J. Nanopart. Res.* **2011**, *13*, 5057–5064. [CrossRef]
53. Schepers, H.E.; van Beek, J.H.G.M.; Bassingthwaighte, J.B. Four methods to estimate the fractal dimension from self-affine signals (medical application). *IEEE Eng. Med. Biol.* **1992**, *11*, 57–64. [CrossRef]
54. Botet, R.; Jullien, R. A theory of aggregating systems of particles: The clustering of clusters process. *Ann. Phys. Fr.* **1988**, *13*, 153–221. [CrossRef]
55. Family, F.; Vicsek, T. Scaling of the active zone in the Eden process on percolation networks and the ballistic deposition model. *J. Phys. A Math. Gen.* **1985**, *18*, L75–L81. [CrossRef]
56. Chauvy, P.F.; Madore, C.; Landolt, D. Variable length scale analysis of surface topography: Characterization of titanium surfaces for biomedical applications. *Surf. Coat. Technol.* **1998**, *110*, 48–56. [CrossRef]
57. Fripiat, I.J.; Gatineau, L.; van Damme, H. Multilayer physical adsorption on fractal surfaces. *Langmuir* **1986**, *2*, 562–567. [CrossRef]
58. Pfeifer, P.; Wu, Y.J.; Cole, M.W.; Krim, J. Multilayer adsorption on a fractally rough surface. *Phys. Rev. Lett.* **1989**, *62*, 1997–2000. [CrossRef] [PubMed]